http://doi.org/10.25130/tjphs.2025.19.2.1.1.22

IRAQI Academic Scientific Journals

Tikrit Journal of Pharmaceutical Sciences

ISSN: 1815-2716 (print) -- ISSN: 2664-231X (online)

Journal Home Page: https://tjphs.tu.edu.iq -- Email: tjops@tu.edu.iq

TJPHS

Synthesis, Characterization, and Molecular Docking Studies of Novel Picolinohydrazide Derivatives as Potential Antibacterial Agents Targeting 1AJ0 Protein

Ali H. Abbas*[1], Istabrick M. Al-Mola[2], Yahya S. Yaseen[1], Mostafa F. Tawfeeq[1], Yaseen S. Hamdoon[3], Riyadh A. Atto AL-Shuaeeb[4]

[1]Department of Pharmaceutical Chemistry, College of Pharmacy, Tikrit University, Tikrit/Salah-Aldin, 34001, Iraq.
[2]Department of Pharmaceutical Chemistry, College of Pharmacy, Mosul University.
[3]Ministry of Health and Environment, Kirkuk Healthcare Directorate, Kirkuk, Iraq.
[4]Department of Pharmacy / Al-Qalam University College, Kirkuk 36001, Iraq.

Keywords:
Picolinohydrazide derivatives, Heterocyclic compounds, Antibacterial agents, Molecular docking, 1AJ0 protein, Structure-based drug design.

Article history:
-Received: 15/11/2025
-Received in revised: 04/12/2025
-Accepted: 05/01/2026
-Available online: 16/01/2026

Corresponding author:
Ali H. Abbas
alih.phchm@tu.edu.iq

Citation:
Abbas A H, Al-Mola I M, Yaseen Y S, Tawfeeq M F, Hamdoon Y S, AL-Shuaeeb R A T. Synthesis, Characterization, and Molecular Docking Studies of Novel Picolinohydrazide Derivatives as Potential Antibacterial Agents Targeting 1AJ0 Protein. Tikrit Journal of Pharmaceutical Sciences. 2025; 19(2):1-22.
http://doi.org/10.25130/tjphs.2025.19.2.1.1.22

Abstract

Background: Bacterial resistance is one of the most immediate problems in healthcare and it requires coordinated efforts for the designing of novel antimicrobial strategies

Objectives: The current study, represents the design and simulation analysis of four novel heterocyclic compounds (4, 7) derived from a sequential three, step methodology.

Materials and Methods: The methodology included acid, catalyzed esterification of picoline, followed by hydrazide formation, and anhydride coupling reactions to obtain the target compounds with the yield ranging from 50% to 60%. The target molecules (4, 7) were structurally specific, as confirmed by ATR, FTIR, ^{1}H, NMR, and ^{13}C, NMR spectroscopic methods. MOE software was used for the simulation of the target molecules to evaluate their binding affinities with 1AJ0 target bacterial proteins, which are the decisive components of metabolic pathways in prokaryotes.

Results: The synthesized molecules (4-7) tested exhibited greater binding affinities, as in the case of compound 7 with, -5.88 Kcal/mol binding affinity, showing a remarkable enhancement of about 31. 5% compared to the control, -4.47 Kcal/mol. This outstanding improvement could be interpreted by the optimal H-bonding with residual ARG A:255, LYS A:221, HIS A:257 and THR A:62, complementary by π-system interactions that reinforce molecular complex stability.

Conclusions: Our findings suggest that the synthesized compounds, particularly compound 7, could serve as valuable lead compounds for developing the next generation antimicrobial agents with improved activity and optimized pharmacokinetic characteristics.

التصنيع والتوصيف ودراسات الالتحام الجزيئي لمشتقات بيكولينوهيدرازيد الجديدة كعوامل محتملة مضادة للبكتيريا تستهدف بروتين1AJ0

علي حسين عباس*[1]، إستبرق محمد المولى[2]، يحيى سعد ياسين[1]، مصطفى فايز توفيق[1]، ياسين سليم حمدون[3]، رياض احمد عطو الشعيب[4]

[1] فرع الكيمياء الصيدلانية، كلية الصيدلة، جامعة تكريت، تكريت/صلاح الدين، 34001، العراق.
[2] فرع الكيمياء الصيدلانية، كلية الصيدلة، جامعة الموصل.
[3] وزارة الصحة والبيئة، مديرية صحة كركوك، كركوك، العراق.
[4] قسم الصيدلة، كلية القلم الجامعة، كركوك 36001، العراق.

الخلاصة

تُعدّ مقاومة البكتيريا للمضادات الحيوية من أبرز التحديات الصحية المُلحة، مما يستدعي اتباع نهج مبتكر لتطوير مضادات الميكروبات. يصف هذا البحث تحضير وتقييم أربع جزيئات حلقية غير متجانسة جديدة (4-7) مُشتقة من بيكولينوهيدرازيد، وذلك من خلال بروتوكول متسلسل من ثلاث خطوات. تم تحليل المركبات بشكل كامل باستخدام تقنيات التحليل الطيفي ATR-FTIR و HNMR[1]و CNMR[13]بدأت استراتيجيتنا التركيبية بعملية الأسترة المحفزة حمضياً، ثم معالجة الهيدرازين، واختُتمت بتفاعلات اقتران الأنهيدرايد، مما أدى إلى إنتاج المركبات النهائية بنسبة مردود تتراوح بين 50 و62%. يُساعد التحليل الحاسوبي باستخدام منصة برنامج MOE في تحديد قوة تفاعل هذه الجزيئات مع البروتين البكتيري 1AJ0، وهو مُكوّن أساسي في آلية التمثيل الغذائي للبكتيريا. أظهرت نتائجنا أن كل مشتق مُصنّع تفوق على الجزيئات المرجعية في قوة الارتباط، حيث حقق المركب 7 الأكثر فعالية طاقة ارتباط بلغت -5.88 كيلو كالوري/مول، مسجلاً تحسناً ملحوظاً بنسبة 31.5% مقارنةً بالرابط المرجعي الذي بلغت طاقته - 4.47 كيلو كالوري/مول. ويعود هذا التحسن في الأداء إلى الروابط الهيدروجينية المثلى مع الأحماض الأمينية المتبقية ARG A:255، وLYS A:221، وHIS A:257، وTHR A:62، والتي تُكمّلها تفاعلات نظام π التي تُعزز استقرار المركب الجزيئي. تشير دراستنا إلى أن هذه البنية القائمة على البيكولينوهيدرازيد قد تُشكل نموذجاً قيماً لعلاجات الجيل القادم من المضادات الحيوية، مع تعزيز استهدافها للهدف وزيادة إمكاناتها السريرية.

الكلمات المفتاحية: مشتقات البيكولينوهيدرازيد، مركبات حلقية غير متجانسة، عوامل مضادة للبكتيريا، الالتحام الجزيئي، بروتين AJ01، تصميم الأدوية القائم على البنية.

Introduction

Despite the existence of modern medicines, infectious diseases brought by bacteria remain a basic threat, with a rapid evolution of a resistance mechanism against all existing therapeutic methods [(1)]. The problem was given top priority by health authorities worldwide concerning antibiotic resistance, thus highlighting the urgent need for research on antibacterial agents with different modes of action [(2)]. The efficacy of existing treatment regimens was diminishing, and it was noticed that there are alarming gaps in antibacterial agents' development in pharmaceutical pipelines [(3)]. These circumstances triggered research designs in the scientific community to move on to something unconventional, with heterocyclic structures identified as very promising scaffolds for their long history with sexes in medicinal design [(4)].

Nitrogen-containing heterocyclic compounds present impressive "versatility in the context of antimicrobial drugs as they are capable of targeting multiple biological substrates through specific modes of interaction" [(5)]. Pyridine-containing compounds call for particular attention owing to the large number of such compounds present in both bioactive compounds of natural origins and marketed drugs today [(6)]. The "picolinic acid series included pyridine carboxylates that exerted broad biological activities in the range of antimicrobial, antifungal, and anticancer agents." The use of hydrazide "groups in such structure has shown particular success since the hydrazides originating from the stable hydrogen bonding networks with target biomolecules conserve desirable physicochemical attributes" [(7)].

Current antibacterial discovery is ever more reliant on virtual prediction algorithms, and molecular docking is now recognized as having an imperative role in virtual predictions concerning binding features prior

to their laboratory preparation [8]. This informatic strategy has evolved as an essential tool in pharmaceutical development, allowing fast screening of very large chemical space datasets and optimization on leads [9]. The mechanistic knowledge on atomic detail about ligand-target engagement informs medicinal chemists to develop leads with superior affinity, extending their selectivity gaps, thereby contributing to improved efficacy [10].

Structure – Designed therapeutic approaches based on the capability to specifically target or find the valid biomolecular structure have shifted the paradigm in drug discovery considerably [11]. The advent of computer-aided predictions coupled with conventional synthesis methods has considerably reduced the time spans for the development of drugs, to the extent that the costs incurred in the search for therapeutic drugs too have been reduced considerably [12]. The present-day systems currently possess the capability to model biological recognition processes at a highly precise level for the identification of drug candidates from large biomolecular libraries [13].

Protein 1AJ0 of bacterial origin has been discovered to be of prime interest because of the essential function it has in the growth of the bacterial cell. This particular protein is engaged in some of the most essential metabolic processes in the bacterium, which are absent in mammals or have very distinct differences. This particular site can be taken as the most ideal location for intervention where little effect would be encountered in the host cell [14]. Creation of the inhibitor protein would generate entirely novel routes through which the resistances would be defeated [15].

Contemporary strategies for the synthesis of the heterocyclic core in the framework of the picolinic acid system revealed a greater emphasis in recent years because of the flexibility of their biological activities as well as their easily accessible routes for synthesis steps [16]. The application of hydrazide derivatives proved highly promising for antibacterial drug development, as indicated by the progress of several candidates in the clinical stages [17]. The optimization of the core structure of the hydrazides using the cyclic anhydride coupling method may be the rational approach in the synthesis of molecular diversity within the framework of the incorporation of essential pharmacophore fragments necessary for the realization of biological activities [18].

Our work initially assumed that the introduction of varied cyclic anhydrides to the picolinohydrazide backbone would allow for the generation of molecules that have high binding affinity towards the bacterial protein 1AJ0. The current research aims include: 1. The generation of a targeted compound library of picolinohydrazides using cyclic anhydride coupling, 2. molecular structure validation using spectroscopic characterization, 3. computer-aided docking studies for determining compound-binding affinity with 1AJ0, and 4. structure-activity relationships to explain the variation in compound affinities. The combined use of traditional compound synthesis and computer-assisted medicinal chemistry research contributes to the ongoing efforts in solving the antimicrobial resistance emergency.

Materials and Methods

Chemical materials and instrumentation

Research -grade chemical reagents and solvents were sourced from established commercial vendors (Sigma-Aldrich, Merck, Fisher Scientific) and utilized without supplementary purification unless explicitly start stated. Starting materials including picolinic acid (≥99%), hydrazine hydrates (≥99%), and cyclic anhydrides – Succinic (≥99%), Malic (≥99%), Glutaric (≥99%), and phthalic (≥99%)- were employed as received. Absolute ethanol underwent pre-treatment via activated molecular sieves 4Å) followed by distillation under inert atmosphere. The solvent 1,4-dioxane received purification through sodium reflex with immediate per-use

distillation. Additional reagents including concentrated sulfuric (95-98%), dichloromethane (≥99.8%), sodium bicarbonate (≥99.7%), and anhydrous magnesium sulfate (≥99.5%) were directly utilized from commercial stocks.

Thermal analysis employed open capillary methodology on Stuart SMP30 apparatus, with the values presented without correction factors. Reaction monitoring and purity assessment utilize thin layer chromatography on silica gel F254 pre-coated plates (0.2 mm, Merck).

Compound visualization occurred under UV illumination (254 nm and 365 nm wavelengths) within a light chamber. Retention coefficients (Rf) were determined and documented for each product.

Infrared spectroscopic analysis employed a Perkin Elmer Spectrum Two FTIR instrument equipped with diamond ATR accessory, scanning 4000-400 cm^{-1} range at 4 cm^{-1} resolution. Individual spectra represented averages of 32 sequential scans, processed via Spectrum software platform. Characteristic vibrational frequencies were identified and reported as wavenumbers (cm^{-1}).

Nuclear magnetic resonance analysis utilized Bruker Avance spectrometers operating at 400-500 MHz for ^{1}H-NMR and 101-126 MHz for ^{13}C-NMR spectroscopy. Deuterated dimethyl sulfoxide (DMSO-d6, 99.9% D) served as solvent with tetramethylsilane (TMS) providing internal reference. Chemical shift values (δ) appear in parts per million (ppm) relative to TMS (δ = 0.00), with coupling constants (J) expressed in Hertz. Signal multiplicity follows standard notation: s (singlet), d (doublet), t (triplet), q (quartet), m (multiplet), dd (doublet of doublets), ddd (doublet of doublet of doublets), br (broad).

Chemical Synthesis

Preparation of Ethyl Picolinate (Compound 2)

Ethyl picolinate was synthesized via a conventional Fischer esterification using sulfuric acid as an acid catalyst. In a typical procedure, picolinic acid (10.0 g, 81.2 mmol) was dissolved in absolute ethanol (70 mL) in a round-bottom flask under magnetic stirring at room temperature until a clear, homogeneous solution was obtained. The reaction mixture was then cooled to about −10 °C using an ice-salt bath, and to this, concentrated sulfuric acid (3 mL, ~56 mmol) was slowly dropwise added with constant stirring. During this process, a white precipitate was formed and observed. The precipitate resulted from protonation at the pyridine nitrogen atom and sulfate salt formation under highly acidic conditions. After the acid addition was completed, the ice, salt bath was removed, and the reaction mixture was allowed to warm to room temperature. The mixture was then heated under reflux at 80 C for 48 hours. In this reaction, the white precipitate dissolution was observed with an increase of temperature, and there was a resulting clear solution, thus showing signs of esterification. The reaction mixture was cooled, and after removal of the excess ethanol, it was dissolved in some distilled water. This was then neutralized to pH 8-9 using aqueous bicarbonate. The formed aqueous part was further extracted using dichloromethane. The organic layers were further washed using water, dried over magnesium sulfate, and filtered. Removal of the solvent under reduced pressure afforded ethyl picolinate as a colorless oil in 70% yield (8.66 g, 57.3 mmol). The product was used directly in subsequent reactions without further purification, and its purity was confirmed by TLC, which showed a single spot (Rf = 0.4) using ethyl acetate–hexane (3:7, v/v) as the mobile phase.

Compound 2 Analytical Data

Physical Form: Colorless oil
Yield: 70% (8.66 g)
Rf: 0.4 (ethyl acetate:hexane, 3:7)
ATR-FTIR (cm^{-1}): 3059 (aromatic C-H stretch), 2981, 2935, 2904, 2873 (aliphatic C-

H stretch of CH_2 and CH_3), 1716 (conjugated ester C=O stretch), 1585 (C=N stretch), 1465, 1438 (aromatic C=C stretch), 1392, 1369 (CH_2 and CH_3 bending), 1172 (ester C-O stretch), 748, 705 (heterocyclic C-H bending)

^{1}H-NMR (500 MHz, DMSO-d6, δ ppm): 8.71 (dd, 1H, J = 1.1, 3.8 Hz, pyridine H), 8.04 (d, 1H, J = 7.8 Hz, pyridine H), 7.98 (t, 1H, J = 7.8 Hz, pyridine H), 7.63 (ddd, 1H, J = 1.1, 4.7, 7.4 Hz, pyridine H), 4.33 (q, 2H, J = 7.1 Hz, OCH_2), 1.31 (t, 3H, J = 7.1 Hz, CH_3)

Preparation of Picolinohydrazide (Compound 3)

Ester-to-hydrazide transformation employed hydrazinolysis methodology, generating the pivotal intermediate for target molecule synthesis. A clean 250 mL round-bottom flask with magnetic stir bar received ethyl picolinate (compound 2, 5.6 g, 37.0 mmol) dissolved in absolute ethanol (40 mL) forming transparent solution. Hydrazine hydrate 99.5% (9.0 mL, 185.0 mmol, five-fold excess) was cautiously introduced dropwise under continuous stirring at ambient conditions. Excess hydrazine ensured reaction completion and compensated for reagent volatility.

Initial stirring occurred at ambient temperature (≈25°C) overnight (12-16 hours) permitting hydrazine nucleophilic attack on ester carbonyl. During this interval, solution color transitioned from colorless to pale pink, characteristic of hydrazide product emergence. Following initial ambient stirring, reflux condenser attachment preceded oil bath heating at 80°C for additional 12 hours with continuous agitation ensuring complete substrate transformation.

Post-reflux, mixture cooling to ambient temperature preceded partial solvent removal (≈20 mL) under reduced pressure via rotary evaporation (water bath: 40°C). Concentrated residue received slow addition to crushed ice beaker (≈100 g) with vigorous stirring, triggering solid product precipitation.

Precipitate collection via vacuum filtration employed Buchner funnel with filter paper, with thorough ice-cold absolute ethanol washing (3 × 10 mL) eliminating impurities and unreacted materials. Crude material underwent recrystallization from 70% aqueous ethanol (v/v) producing pure picolinohydrazide as off-white crystalline needles. Recrystallization involved dissolving crude product in minimal hot 70% ethanol, permitting slow ambient cooling, then ice bath placement maximizing crystallization. Purified crystals underwent filtration, cold 70% ethanol washing, and vacuum desiccator drying over anhydrous calcium chloride for 24 hours.

Compound 3 Analytical Data

Physical Form: Off-white crystals
Yield: 80% (4.06 g, 29.6 mmol)
Melting Point: 98-100°C
Rf: 0.85 (methanol:dichloromethane, 1:9)
ATR-FTIR (cm^{-1}): 3363 (secondary amide N-H stretch), 3290, 3209 (primary amine N-H stretch), 3016 (aromatic C-H stretch), 1670 (amide C=O stretch, amide I band), 1647 (N-H bending), 1593 (C=N stretch), 1566 (amide II band N-H bending), 1516, 1469, 1431 (aromatic C=C stretch), 1246 (C-N stretch), 752, 702 (heterocyclic C-H bending)

^{1}H-NMR (500 MHz, DMSO-d6, δ ppm): 9.89 (br s, 1H, hydrazide NH), 8.60 (br d, 1H, J = 3.8 Hz, pyridine H), 7.96-8.00 (m, 2H, pyridine H), 7.56 (br t, 1H, J = 5.5 Hz, pyridine H), 4.61 (br s, 2H, NH_2).

General Synthetic Protocol for Target Compounds 4-7

Target molecule synthesis proceeded via picolinohydrazide reaction with diverse cyclic anhydrides following standardized methodology. Each preparation began with precise picolinohydrazide weighing (compound 3, 0.25 g, 1.822 mmol) transferred to clean, dry 50 mL round-bottom flask. Anhydrous 1,4-dioxane (5 mL) dissolution under magnetic stirring at ambient conditions produced clear solution.

Appropriate cyclic anhydride (1.822 mmol, equimolar quantity) received single-portion

solid addition. Specific reagents comprised: (A) succinic anhydride (0.1824 g) generating compound 4, (B) maleic anhydride (0.178 g) producing compound 5, (C) glutaric anhydride (0.2079 g) yielding compound 6, and (D) phthalic anhydride (0.267 g) forming compound 7.

After the addition of the anhydride, the room agitation continued for some 5 minutes to achieve complete dissolution. The reaction mixtures were subjected to reflux heating using a reflux condenser attachment at 100-105°C. This corresponds to the boiling point of dioxane. This process was continued for 4 hours while. Reflux period witnessed product formation evidenced by precipitate appearance in selected cases or solution color modifications.

Post-reflux, mixtures cooled to ambient temperature, then received additional ice bath cooling for 30 minutes maximizing product precipitation. Solid collection via vacuum filtration employed Buchner funnel, with thorough cold distilled water washing (3 × 10 mL) eliminating unreacted anhydride or solvent, followed by cold ethanol washing (2 × 5 mL). Crude materials underwent recrystallization from 50% aqueous ethanol

(v/v): crude solid dissolution in minimal hot 50% ethanol, hot filtration removing insoluble materials, slow ambient cooling, then ice bath placement. Pure crystals received filtration, cold 50% ethanol washing, and vacuum desiccator drying over anhydrous calcium chloride for 24 hours preceding characterization.

The complete synthetic pathway from picolinic acid to final target compounds 4-7 is illustrated in Figure 1. This multi-step approach provides efficient access to structurally diverse picolinohydrazide derivatives through systematic variation of the cyclic anhydride coupling partner. The reaction sequence demonstrates excellent reproducibility and scalability, yielding compounds in moderate to good yields (50-62%) suitable for comprehensive biological evaluation and computational docking studies.

Individual Compound Characterization

Compound 4: N'- (Pyridin-2-ylcarbonyl) succinohydrazide analog

Derived from Picolinohydrazide -succinic anhydride coupling.

Physical Form: White powder

Yield: 62% (0.267 g)

Melting Point: 184-187°C

Rf: 0.2 (methanol:dichloromethane, 2:8)

Molecular Formula: $C_{10}H_{11}N_3O_4$

Molecular Mass: 237.21 g/mol

ATR-FTIR (cm^{-1}): 3321 (amide N-H stretch), 3059 (aromatic C-H stretch), 1724, 1693, 1639 (C=O stretches), 1570 (C=N stretch), 1523, 1492 (aromatic C=C stretch), 752, 702 (heterocyclic C-H bending)

^{1}H-NMR (400 MHz, DMSO-d6, δ ppm): 12.14 (s, 1H), 10.40 (s, 1H), 10.07 (s, 1H), 8.67 (d, J = 4.9 Hz, 1H), 8.01 (t, J = 6.2 Hz, 2H), 7.63 (dq, J = 8.0, 4.1 Hz, 1H)

^{13}C-NMR (101 MHz, DMSO-d6, δ ppm): 174.02, 170.44, 162.98, 149.59, 149.10, 138.41, 138.30, 127.41, 122.75, 29.30, 28.61

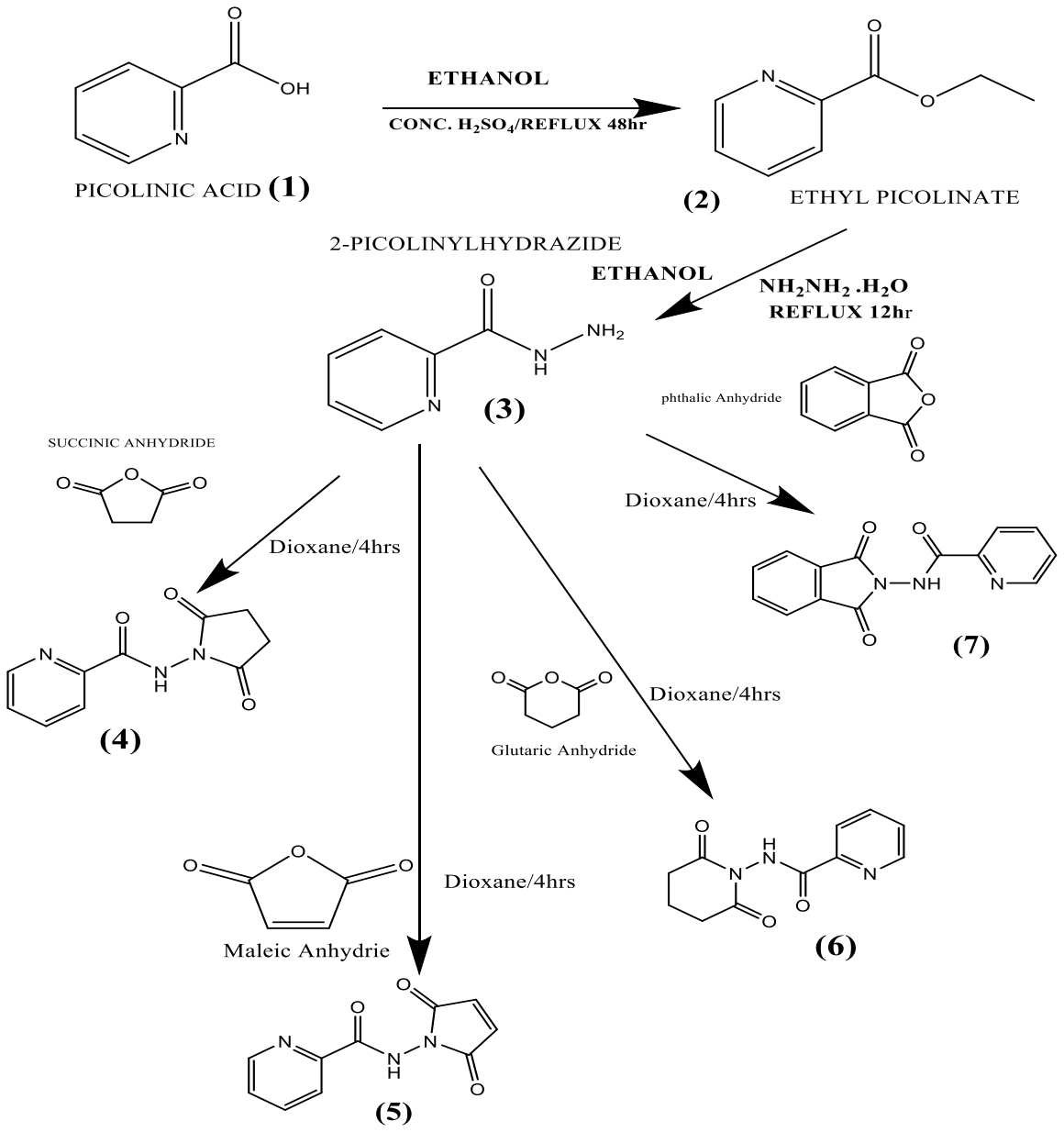

Figure 1. Synthetic route for preparation of picolinohydrazide derivatives 4-7. Reagents and conditions: (i) Picolinic acid (1), absolute EtOH, conc. H_2SO_4, reflux, 80°C, 48h, yield 70%; (ii) Ethyl picolinate (2), $N_2H_4 \cdot H_2O$ (5 equiv.), absolute EtOH, reflux, 80°C, 12h, yield 80%; (iii) Picolinohydrazide (3), cyclic anhydride (succinic, maleic, glutaric, or phthalic anhydride), 1,4-dioxane, reflux, 100-105°C, 4h, yields 50-62%.

Compound 5: N'-(Pyridin-2-ylcarbonyl) maleohydrazide analog
Derived from picolinohydrazide-maleic anhydride coupling.
Physical Form: Off-white crystalline powder
Yield: 50% (0.213 g)
Melting Point: 195-198°C
Rf: 0.3 (methanol:dichloromethane, 2:8)
Molecular Formula: $C_{10}H_9N_3O_4$
Molecular Mass: 235.20 g/mol
ATR-FTIR (cm^{-1}): 3321 (amide N-H stretch), 3032 (aromatic C-H stretch), 1732, 1689, 1666 (C=O stretches), 1612 (C=N stretch), 1585, 1566, 1504 (aromatic C=C and alkene C=C stretches), 752, 700 (heterocyclic C-H bending)

^{1}H-NMR (500 MHz, DMSO-d6, δ ppm): 12.10 (s, 3H), 10.70 (s, 2H), 8.67-8.72 (m, 1H), 8.65 (s, 0H), 8.00-8.11 (m, 3H), 7.67 (ddd, J = 6.9, 4.8, 2.3 Hz, 1H), 6.45 (d, J = 12.2 Hz, 1H), 6.41 (s, 1H), 6.35 (d, J = 12.2 Hz, 1H)

^{13}C-NMR (126 MHz, DMSO-d6, δ ppm): 167.42, 163.23, 162.78, 149.28, 149.19, 138.42, 133.98, 127.62, 126.91, 122.87

Compound 6: N'-(Pyridin-2-ylcarbonyl)glutarohydrazide analog
Derived from picolinohydrazide-glutaric anhydride coupling.
Physical Form: White crystals
Yield: 55% (0.251 g)
Melting Point: 140-143°C
Rf: 0.15 (methanol:dichloromethane, 2:8)
Molecular Formula: $C_{11}H_{13}N_3O_4$
Molecular Mass: 251.24 g/mol
ATR-FTIR (cm^{-1}): 3325 (amide N-H stretch), 3055 (aromatic C-H stretch), 1728, 1689, 1678 (C=O stretches), 1589 (C=N stretch), 1570, 1535, 1500 (aromatic C=C stretch), 748, 705 (heterocyclic C-H bending)
^{1}H-NMR (500 MHz, DMSO-d6, δ ppm): 12.07 (s, 1H), 10.41 (s, 1H), 9.97-10.01 (m, 1H), 8.65-8.70 (m, 1H), 7.95-8.09 (m, 2H), 7.64 (ddd, J = 6.9, 4.8, 2.4 Hz, 1H), 2.32 (t, J = 7.5 Hz, 2H), 2.17-2.27 (m, 2H), 1.79 (p, J = 7.5 Hz, 2H)

^{13}C-NMR (126 MHz, DMSO-d6, δ ppm): 174.67, 171.14, 163.18, 149.63, 149.08, 138.30, 127.41, 122.77, 33.26, 32.87, 20.97

Compound 7: N'-(Pyridin-2-ylcarbonyl) phthalic hydrazide analog
Derived from picolinohydrazide-phthalic anhydride coupling.
Physical Form: Off-white powder
Yield: 56% (0.289 g)
Melting Point: 218-221°C
Rf: 0.66 (methanol:dichloromethane, 3:7)
Molecular Formula: $C_{14}H_{11}N_3O_4$
Molecular Mass: 285.26 g/mol
ATR-FTIR (cm^{-1}): 3286 (amide N-H stretch), 3047 (aromatic C-H stretch), 1797, 1732, 1678 (C=O stretches), 1616 (C=N stretch), 1589, 1570, 1485 (aromatic C=C stretch), 752, 709 (heterocyclic C-H bending)
^{1}H-NMR (500 MHz, DMSO-d6, δ ppm): 11.43 (d, J = 1.4 Hz, 1H), 8.79 (dt, J = 4.8, 1.4 Hz, 1H), 8.08-8.17 (m, 2H), 7.92-8.06 (m, 4H), 7.93 (s, 1H), 7.76 (td, J = 5.1, 3.6 Hz, 1H)

^{13}C-NMR (126 MHz, DMSO-d6, δ ppm): 165.53, 163.77, 149.48, 148.28, 138.65, 135.92, 129.89, 128.29, 124.34, 123.43

Computational Docking Studies
Ligand Structure Preparation
Two-dimensional molecular architectures of synthesized compounds (4-7) were constructed employing ChemDraw Professional version 20.0 (PerkinElmer Informatics). Structures received careful design based on spectroscopic validation and established reaction pathways. Each architecture underwent verification for proper atomic connectivity, bond order accuracy, and stereochemical assignments where relevant.
Planar structures underwent transformation to three-dimensional geometries with MOL format export (.mol). Ligand energy minimization employed Molecular Mechanics Force Field (MMFF94x) within MOE software obtaining thermodynamically favorable conformations. Minimization proceeded with 0.001 kcal/mol/Å^2 gradient convergence criterion. Optimized structures advanced to docking investigations.

Protein Structure Preparation

Three-dimensional crystallographic coordinates of bacterial protein 1AJ0 originated from RCSB Protein Data Bank repository (http://www.rcsb.org) in PDB format. Structure import into Molecular Operating Environment (MOE) version 2022.02 (Chemical Computing Group, Montreal, Canada) enabled preparation and docking analysis [19].

Preparation protocol encompassed multiple essential steps ensuring result reliability. Initially, crystallographic water molecules underwent removal, as these can disrupt ligand accommodation and amplify computational demands. Co-crystallized ligand present in original PDB file received temporary removal yet separate retention for subsequent comparative docking analysis serving as reference compound.

Hydrogen atom addition to protein architecture employed Protonate 3D functionality within MOE, assigning optimal protonation states to ionizable residues based on predicted pKa values at physiological pH (7.4). This procedure proves critical because residue protonation states profoundly influence electrostatic recognition with ligands [20]. Protein architecture then received energy minimization via Amber10: EHT force field relieving steric tensions and refining geometry. Minimization employed 0.01 kcal/mol/Å² gradient convergence, with heavy atom tethering at 10 kcal/mol/Å² force constant preventing excessive structural deviation from crystallographic coordinates.

Active Site Definition

Protein 1AJ0 active site identification relied on co-crystallized ligand positioning within original PDB coordinates. Binding cavity definition encompassed all residues within 10 Å spherical radius from co-crystal ligand geometric center. This domain received careful examination for key residue presence recognized as important for ligand accommodation including charge residue (ARG, LYS, GLU, ASP), hydrogen bonding participants (SER, THR, TYR, HIS), and hydrophobic residues (PHE, TRP, LEU, VAL, ILE).

MOE site finder module enabled computational identification and characterization of potential binding locations with results compared against crystallographic site ensuring consistency. Active site received three-dimensional visualization using MOE rendering tools understanding special residue organization and identifying potential interaction sites for designed ligands [21].

Docking Simulation Protocol

Docking simulations were done with the MO-Dock tool in MOE 2022.02. The Triangle Matcher algorithm fit poses, checking several binding poses by overlapping sets of three ligand atoms onto sets of three receptor site points Receptor site points came from alpha spheres at possible binding sites in the active receptor cavity. Each ligand was run 30 times in separate docking simulations to search the conformational space well enough. The London dG scoring function made early estimates of binding free energy during placement [22]. After placement, poses were improved with an induced fit method. This allowed flexibility in both the ligand and nearby protein side chains within 4.5 Å of the ligand. This refinement stage is key for seeing conformational changes when a ligand binds.

The final scoring of the refined pose used the GBVI/WSA dG scoring function. This function estimates how well a molecule binds by looking at van der Waals forces, electrostatic interactions, and how the molecule interacts with the solvent [23]. Poses were ranked by binding energy scores (kcal/mol); a lower value suggests a stronger predicted affinity.

To confirm the docking protocol, the co-crystal ligand was re-docked into the active site and the predicted binding arrangement was matched with the crystallographic pose. The root mean square deviation (RMSD) was calculated to measure how well the predicted and actual configurations matched. An RMSD value less than 2.0 Å was considered acceptable [24].

Interaction Pattern Analysis

Optimal scoring docking poses for each synthesized compound and co-crystal ligand received selection for comprehensive interaction examination. MOE ligand interactions utility enabled identification and visualization of all intermolecular contacts between ligands and protein binding cavity. Analysis encompassed hydrogen bond identification (3.5Å distance threshold, 120° angle threshold), ionic contacts π-π stacking, π-cation interactions, and hydrophobic association [25].

Hydrogen bonding patterns underwent detailed analysis identifying critical donor-acceptor partnerships and evaluating their stabilizing contributions. Individual hydrogen bond geometry and strength received assessment based on donor-acceptor spacing and angular parameters. Hydrophobic interactions received evaluation based on non-polar ligand atom proximity to hydrophobic protein residues. Two-dimensional interaction schematics were generated providing transparent representation of all contacts for each ligand-protein assembly.

Binding energies from docking investigations were compiled and compared across all compounds establishing structure-activity correlations. Statistical examination correlated structural compound features with predicted affinity profiles

Results and Discussion

Synthetic Chemistry and Structural Validation

We made four new picolinohydrazide derivatives (compounds 4-7) using a three-step process. The process started with an acid-catalyzed esterification, continued with a hydrazine-mediated change to form the key intermediate, and ended with cyclic anhydride coupling to get the final products. We picked this method as it is simple, gives the same results each time, and lets us make different structures by picking different anhydride components.

Ethyl Picolinate Synthesis and validation (Compound 2).

The esterification reaction using absolute ethanol was quite effective, resulting in about 70% conversion to ethyl picolinate. The appearance of white precipitate when adding the catalyst, which dissolves on heating, is related to protonation of the pyridine nitrogen, forming sulfate salt. This agrees with established reactions involving pyridine derivatives, which readily protonate under an acidic atmosphere because their basic nitrogens readily protonate [26].

Infrared analysis of compound 2 showed characteristic absorptions, which authenticated the successful formation of the ester. The prominent absorptions found at 1716 cm−1, due to the C=O stretching in the conjugated ester, together with the C-O stretching band at 1172 cm−1, provided conclusive evidence on the formation of the ester functional group. The characteristic stretching absorptions due to C-H in the aromatic rings were found at 3059 cm−1, while those due to C-H in the ethyl group appeared at 2981, 2935, 2904, and 2873 cm−1. The integrity of the pyridine rings in the compound was confirmed

The structure validation information obtained by 1H-Proton NMR spectroscopy included the presence of pyridine aromatic protons showing a distract signal in the range 7.63-8.71 ppm. Typical ester ethyl resonances given by quartet and triplet patterns in the 4.33 ppm region (J=7.1 Hz) and 1.31 ppm region (J=7.1Hz), respectively, absolutely proved the existence of the -OCH2CH3 group.

Picolinohydrazide Synthesis and Validation (Compound 3)

Ester transformation to hydrazide via hydrazinolysis achieved exceptional 80% conversion, evidencing hydrazine hydrate's potent reactivity toward star functionalities. Five-fold hydrazine excess guaranteed complete substrate transformation and accommodated the agent volatility. Solution

color evolution from colorless to pale pink throughout reaction typifies hydrazide generation and parallels observation in analogous systems documented in scientific literature [27].

Infrared spectroscopical profile of compound 3 exhibit multiple characteristic band substantiating successful ester to hydrazide conversion. Ester Carbonyl absorption disappearance at 1716 cm^{-1} coupled with amide carbonyl emergence at 1670 cm^{-1} (amide I signature) furnished primary transformation evidence. Supplementary N-H stretching vibrations at 3363 cm^{-1} (secondary amide) and 3290,3209 cm^{-1} (primary amine) verified hydrazide functionalities (-CONHNH2) presence. Amide II band appearance at 1566 cm^{-1}, originating from coupled N-H bending and C-N stretching, provided additional hydrazide structural support.

Proton NMR spectrum displayed broad singlet at 9.89 ppm assigned to hydrazide NH proton, with another broad singlet at 4.61 ppm corresponding to NH_2 protons. Pyridine aromatic protons materialized at anticipated positions spanning 7.56-8.60 ppm. Selected signal broadening, particularly exchangeable protons, correlates with hydrogen bonding phenomena in DMSO medium. Comprehensive spectroscopic data demonstrated excellent agreement with theoretical picolinohydrazide structure, verifying identity and purity.

Target Compound Synthesis and Validation (4-7)

Terminal synthetic sequence involved picolinohydrazide coupling with four distinct cyclic anhydrides (succinic, maleic, glutaric, phthalic) generating target compounds 4-7. This transformation proceeds via terminal NH_2 group nucleophilic attack on anhydride carbonyl carbon, followed by ring-opening yielding products bearing both amide and carboxylic acid moieties. Reaction conversions spanned 50-62%, representing satisfactory performance for this transformation class considering potential side pathways and bis-acylation possibilities.

Comprehensive spectroscopic characterization employing ATR- FTIR, ^{1}H-NMR, and ^{13}C-NMR confirmed all synthesized compound structures. Infrared spectroscopic profile for compounds 4-7 uniformly displayed characteristic signatures consistent with proposed architectures. Note the general occurrence of multiple carbonyl absorptions between 1639-1797 cm-1 due to the concurrent presence of carboxylic acid carbonyl and amide carbonyl. The N-H stretching absorptions occurred between 3286-3325 cm-1, indicating the occurrence of the amide linkage. The Pyridine ring C=N absorption occurred in all samples between 1570-1616.

Proton NMR Spectra: Proton NMR spectra provided conclusive information on molecular structures based on distinct spectral patterns. The exchangeable proton signals due to carboxylic acid and amide groups appeared as downfield signals (10-12 ppm), whereas the aromatic proton signals of pyridine groups showed signals at (7.5-8.8) ppm. The aliphatic chain proton signals in compounds 4,5, and 6 were found as expected in upfield regions (1.8-2.4) ppm.

Carbon-13 NMR spectroscopy was very important in determining the validity of certain structures based on typical values for certain groups. The carbonyl carbons were differentiated into distinct ranges. For carboxylic acids, it was 165-175 ppm, while for amides, it was 162-171 ppm. The aromatic carbons of the pyridine ring appeared at 122-150 ppm, while aliphatics were seen at 20-34 ppm. The number of carbons detected was far lower compared to theory values, establishing symmetry. Compound 4 showed eleven carbons, which established it as C10. Compound 5 showed ten carbons, which established it as an unsaturated C10. Compound 6 showed eleven carbons, which established it as C11. Compound 7 manifested ten aromatic carbon signals characteristic for its condensed aromatic C_{14} framework.

Successful preparation and exhaustive multi-technique characterization of all four targeted structures furnished appropriate material for subsequent computational docking investigations and established foundation for structure-activity correlation analysis.

Computational Docking Investigations

Protocol Validation

Docking protocol underwent validation through co-crystal ligand re-docking into 1AJ0 protein active cavity. Docking geometry comparison with crystallographic positioning yielding roots means square deviation (RMSD) of 1.23 Å. This value resides comfortably within acceptable validation parameters (RMSD less than 2 Å), demonstrating that docking parameter and scoring algorithms employed in our investigation accurately reproduce experimentally determined binding geometries. This validation phase instills confidence in predicted binding pose reliability for synthesized compounds

Binding energy Evaluation

Computational docking investigations evaluate binding affinity of compounds 4-7 toward bacterial protein 1AJ0 with performance comparison against co-crystal reference. Binding energies derived via GBVI/WSA dG scoring algorithm appear in Table 1. All four synthesized derivatives manifested more favorable (increasingly negative) binding energies relative to co-crystal ligand, implying superior target protein affinity [28].

Table 1: Comparative Binding Energy Analysis

Molecular Entity	Binding energy (kcal/mol)	Enhancement vs Reference	Percentage Gain (%)
Co-Crystal Reference	-4.47	-	-
Compound 4	-5.43	-0.96	21.5
Compound 5	-5.25	-0.78	17.4
Compound 6	-5.66	-1.19	26.6
Compound 7	-5.88	-1.41	31.5

Reference Co-crystal legend registered binding energy of -4.47kcal/mol, setting up the comparative datum point. Compound4 showed binding energy of -5.43kcal/mol, denoting 21.5% increase in affinity. Compound5 showed binding energy of -5.25kcal/mol, denoting 17.4% increase. Compound6 showed binding energy of -5.66kcal/mol, denoting 26.6% increase. Notably, compound7 showed optimized binding energy of -5.88kcal/mol denoting considerable improvement of 31.5%.

Binding energy progression (7 > 6 > 4 > 5 > co-crystal reference) unveils intriguing structure-activity correlations. Compound 7 incorporation aromatic phthalic part, having maximum binding affinities, implying that incorporation of supplementary aromatic cycle enhances interactions at protein binding sites, presumably because of π-π stacking or increased hydrophobic interactions [29]. Compound 6, having a glutaric chain with five carbons, having secondary affinities, implying that aliphatic moieties with extended chains provide superior geometry and compatibility at the binding pockets. Compound 4, having a succinic group with four carbons, having intermediate affinities, and Compound 5 with unsaturated maleic parts, had lowest affinities amongst all synthesized compounds but still better than the co-crystal reference.

Even though compound 5 has a C=C double bond that should make it stiffer and bind better, it doesn't bind as well as compound 4. This suggests the double bond might be forcing it into a shape that doesn't fit the binding pocket very well. So, being able to change shape seems pretty important for getting the best binding.

Interaction Analysis of Co-Crystal and Synthesized Compounds.

Co-Crystal Ligand Interaction Profile

Comprehensive examination of co-crystal ligand binding mode revealed multiple key interactions stabilizing its association with 1AJ0 protein active site (Figure 2A, Figure 3A). The reference ligand established conventional hydrogen bonds with two critical residues: ARG A:255 (2.02 Å) and

HIS A:257 (2.57 Å). The positively charged arginine residue furnished robust electrostatic stabilization via its guanidinium functionality, while histidine contributed binding through imidazole side chain interactions. Beyond conventional hydrogen bonding, the co-crystal ligand participated in π-sulfur interactions with ARG A:63 (4.35 Å) and π-alkyl interactions with LYS A:221 (5.23 Å). These interactions collectively contributed to the observed binding energy of -4.47 kcal/mol. However, the relatively modest binding energy implies incomplete optimization of all potential binding pocket interaction points, permitting improvement through rational design [30].

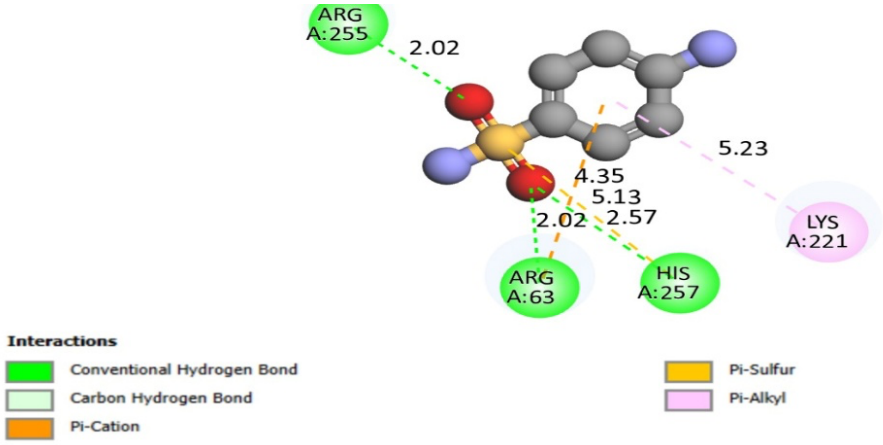

2A

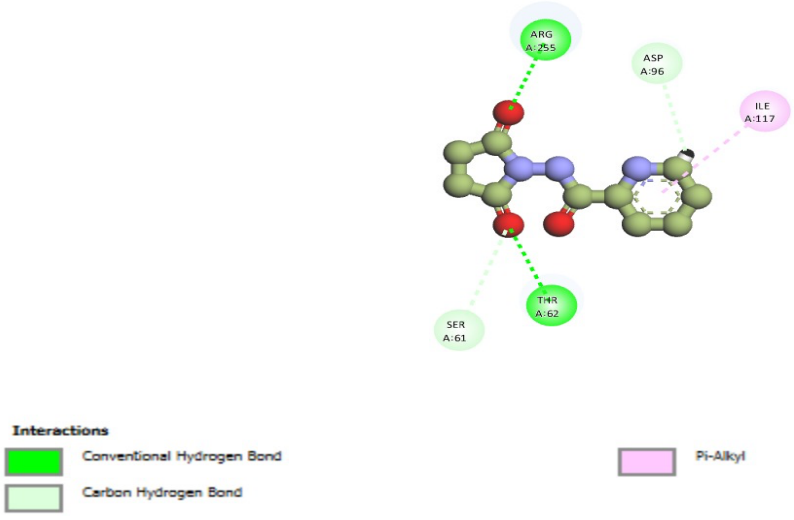

2B

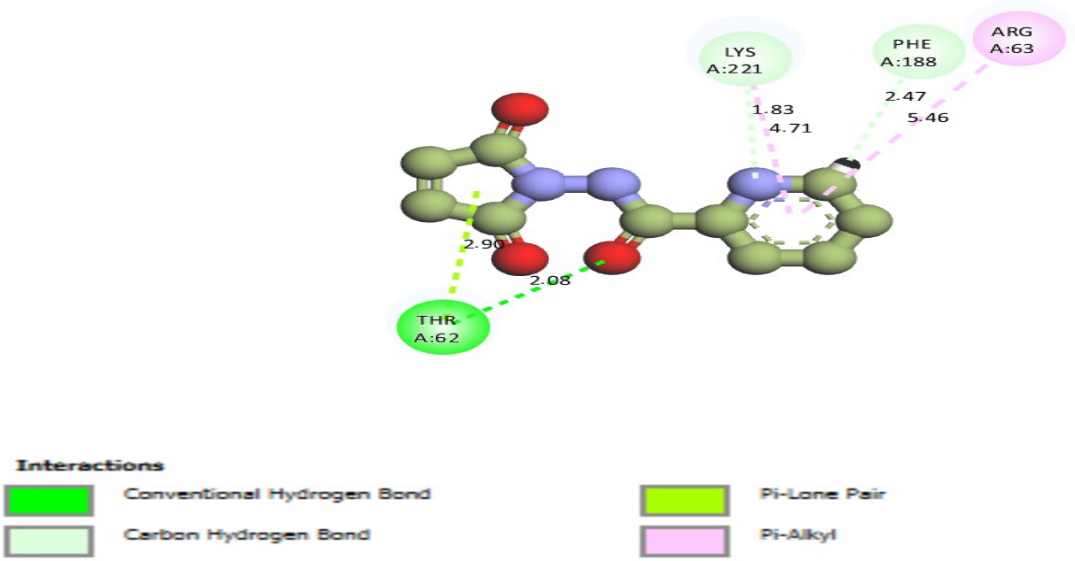
LYS
A:221
PHE
A:188
ARG
A:63
1.83
4.71
2.47
5.46
2.90
2.08
THR
A:62
Interactions
Conventional Hydrogen Bond
Carbon Hydrogen Bond
Pi-Lone Pair
Pi-Alkyl

2C

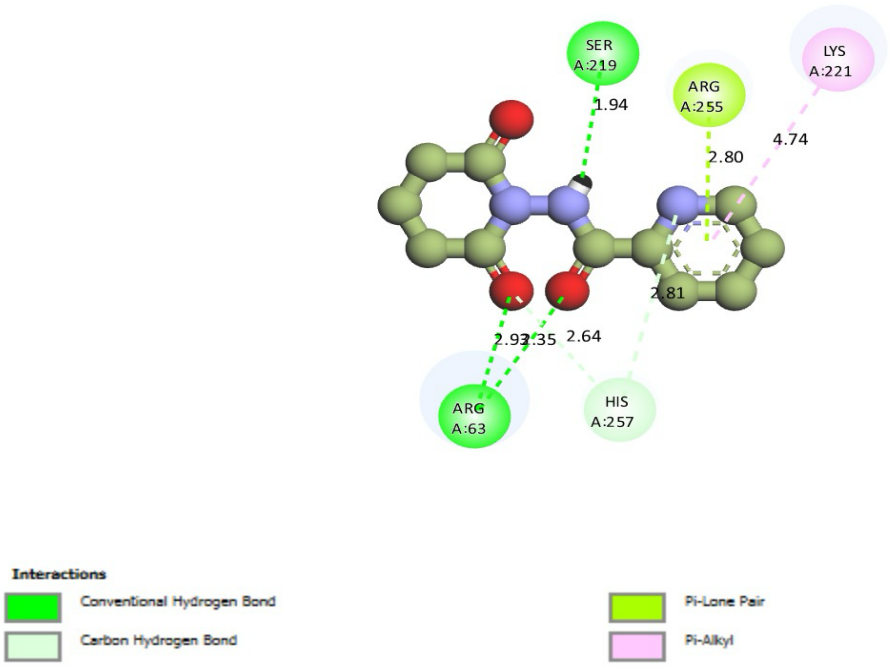
SER
A:219
ARG
A:255
LYS
A:221
1.94
2.80
4.74
2.81
2.93
3.35
2.64
ARG
A:63
HIS
A:257
Interactions
Conventional Hydrogen Bond
Carbon Hydrogen Bond
Pi-Lone Pair
Pi-Alkyl

2D

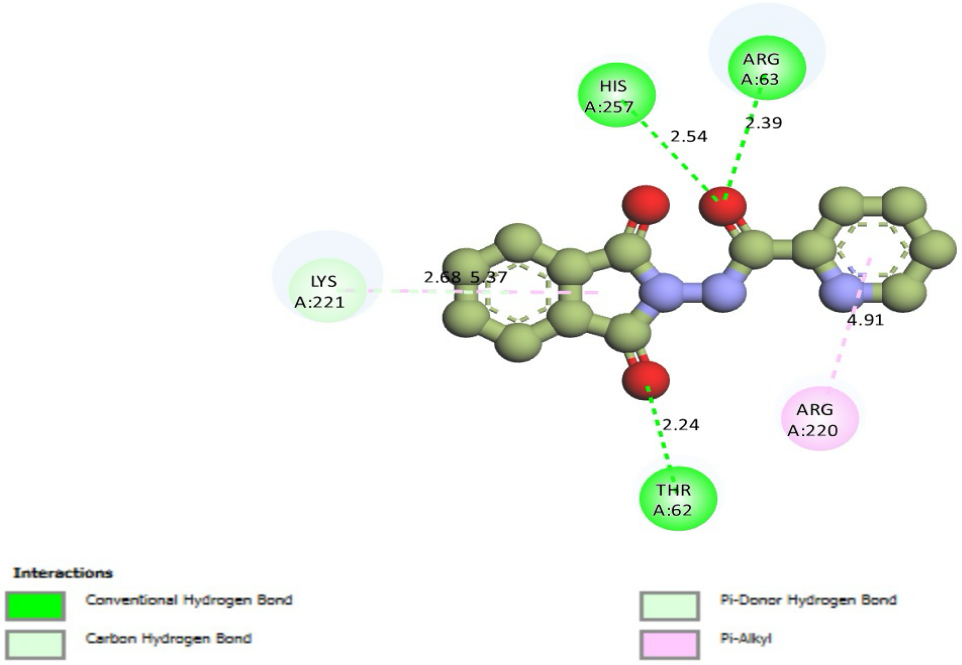

2E

Figure 2. Two-dimensional interaction diagrams of docked compounds with bacterial protein 1AJ0 active site. (A) Co-crystal reference ligand showing conventional hydrogen bonds with ARG A:255 and HIS A:257, π-sulfur interaction with ARG A:63, and π-alkyl interaction with LYS A:221. (B) Compound 4 displaying hydrogen bonds with ARG A:255, THR A:62, HIS A:257, and ARG A:63. (C) Compound 5 exhibiting hydrogen bonds with ARG A:255, THR A:62, and HIS A:257, along with π-alkyl interactions. (D) Compound 6 showing hydrogen bonds with THR A:62, LYS A:221, and interactions with PHE A:188 and ARG A:63. (E) Compound 7 demonstrating hydrogen bonds with THR A:62, HIS A:257, ARG A:63, and π-alkyl interaction with ARG A:220. Green dashed lines indicate conventional hydrogen bonds, pink dashed lines represent π-alkyl interactions, yellow dashed lines show π-sulfur interactions, and light green dashed lines denote π-lone pair interactions. Distance measurements are shown in Ångströms (Å).

Compound 4 Interaction Profile

Compound 4 established comprehensive interaction architecture within 1AJ0 active site, as depicted in Figure 2B and Figure 3B. Conventional hydrogen bonds formed with ARG A:255 (1.94 Å) and THR A:62 (2.64 Å and 2.35 Å), accompanied by interactions with HIS A:257 (2.64 Å) and ARG A:63 (2.93 Å). The lysine residue LYS A:221, with its extended flexible side chain terminated by positively charged amino group, established favorable π-alkyl interactions (4.74 Å). Additionally, compound 4 engaged in hydrophobic contacts with SER A:219 and exhibited π-lone pair interactions, collectively contributing to the -5.43 kcal/mol binding energy. The succinyl moiety appears furnishing appropriate chain length positioning carboxylic acid for optimal hydrogen bonding while maintaining favorable picolinohydrazide core-protein surface contacts.

Compound 5 Interaction Profile

Compound 5, which has an unsaturated maleic part, binds with an energy of -5.25 kcal/mol, and the specific way it interacts is shown in Figures 2C and 3C. Our analysis showed that it forms hydrogen bonds with ARG A:255 (2.80 Å), THR A62 (2.8 Å), and HIS A:257. Other contacts include ARG A:63 (2.81 Å), a π- alkyl interaction with LYS A :221 (4.74 Å), and ARG A:220. The contact with THR A:62 is special because it's not seen in the co-crystal ligand, meaning that the way compound 5 is built allows it to reach an extra binding area. Still, the maleic part with its C=C double bond creates shape limitations that might stop the best positioning of interacting groups. The flat shape caused by the double bond decreases how much the compound can change its shape, which might limit how well it fits into the binding pocket.

Compound 6 Interaction Profile

Compound 6 showed a binding energy of -5.66 kcal/mol, making it the second-best binder we created. You can see how it binds in Figures 2D and 3D.

The glutaryl part, with its five-carbon chain, seemed to give it just the right amount of flexibility to reach into the binding pocket. It created hydrogen bonds with THR A:62 (at distances of 2.90 Å and 2.08 Å), LYS A:221 (at 1.83 Å), and interacted with PHE A:1 (at 2.47 Å, 4.71 Å, and 5.46 Å) and ARG A:63. Plus, it had a π-alkyl interaction that helped keep it stable.

It bound better than compound 4 (which has a four-carbon chain). This suggests that those extra methylene units in the glutaryl part let it

fit the binding pocket better. The longer chain might let the carboxylic acid at the end get deeper into the binding site or position itself to make stronger hydrogen bonds. Because the five-carbon chain is flexible, compound 6 can change its shape to fit the binding site while still interacting well with it.

Compound 7 Interaction Profile

Compounds have been emerged as optimal performer within -5.88 kcal/mol binding energy, representing 31.5% enhancement over co-crystal reference, as visualize in Figure 2E and Figure 3E. The phthalic moiety presence introduces aromatic ring significantly amplifying binding through multiple mechanisms. Hydrogen bonds formed with THR A:62 (2.24 Å and 2.39 Å), HIS A:257 (2.54 Å), and ARG A:63 (2.39 Å), establishing stable electrostatic interaction network. The compound engaged in π-alkyl interactions with ARG A:220 (4.91 Å) and maintained contacts with LYS A:221. Beyond conventional hydrogen bonds, compound 7 likely benefits from supplementary π-π stacking interactions between phthalic aromatic ring and binding pocket aromatic residues [31]. The significantly improved binding energy strongly implicates aromatic stacking contribution. The phthalic ring additionally increases overall molecular hydrophobicity, enhancing van der Waals interactions with hydrophobic residues lining binding pocket. The rigid aromatic phthalic system furnishes well-defined geometric framework potentially orienting pharmacophoric groups optimally for maximum binding.

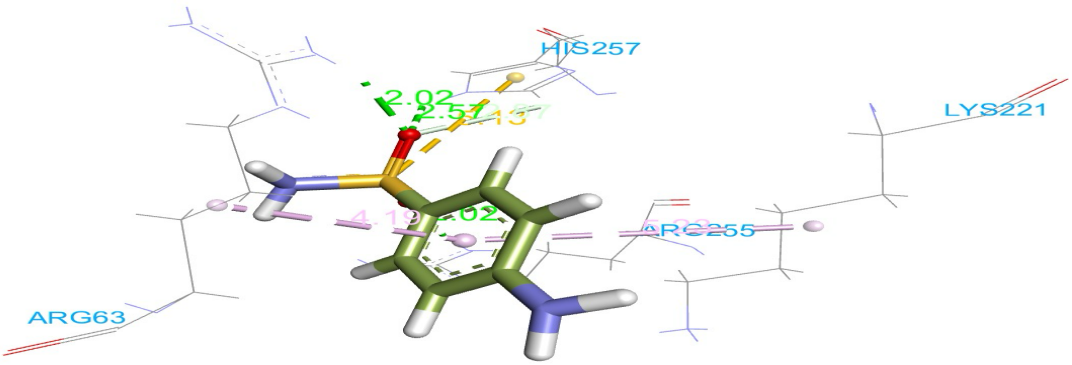

3A

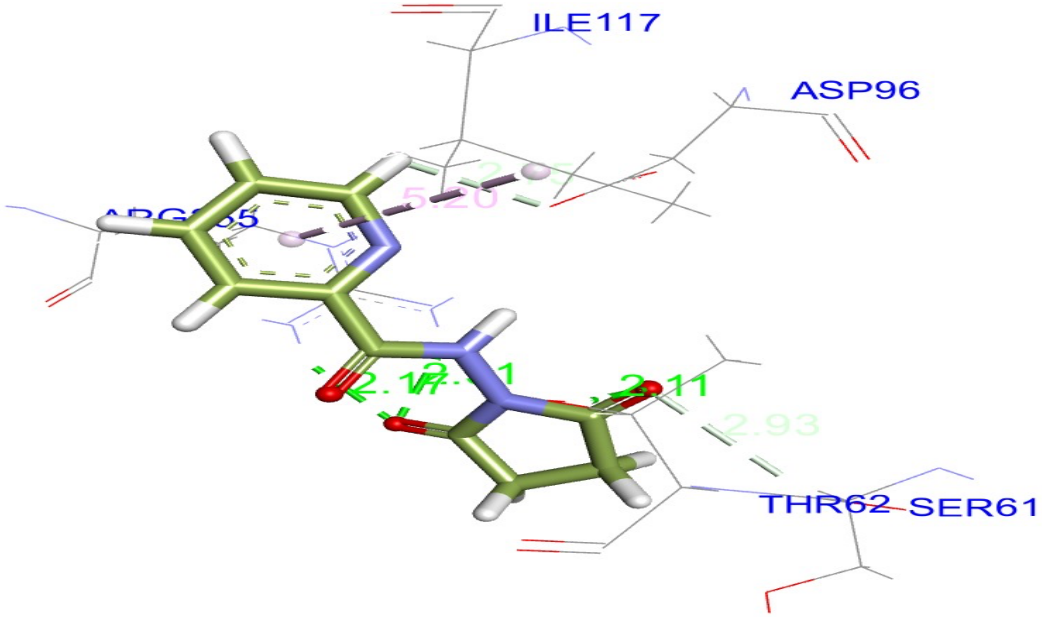

3B

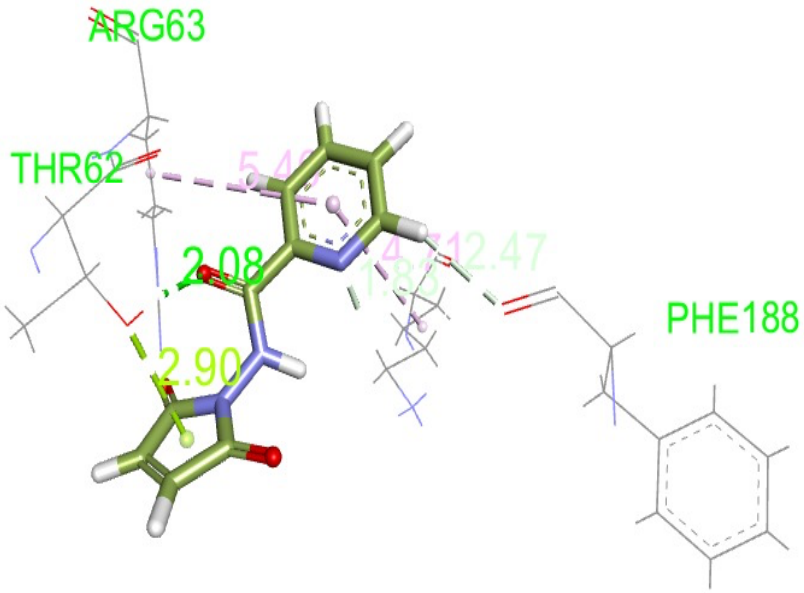
ARG63
THR62
2.08
2.90
PHE188

3C

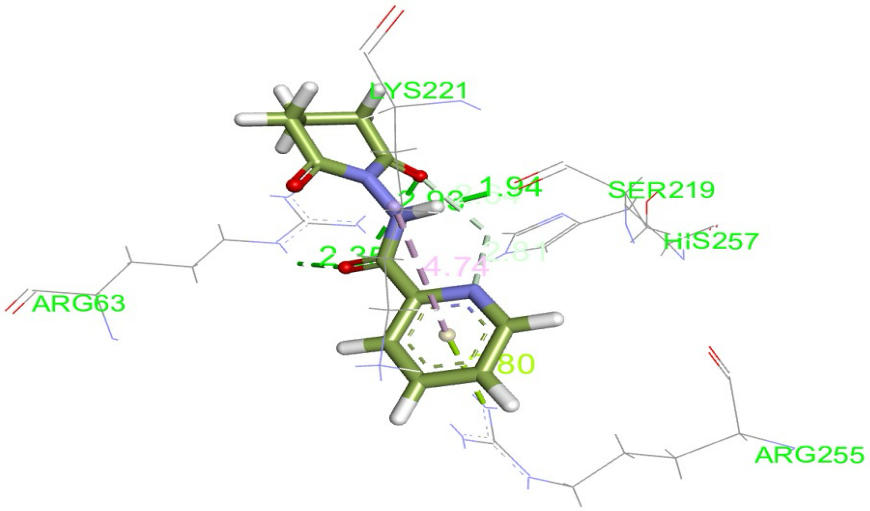
LYS221
1.94
SER219
HIS257
ARG63
ARG255

3D

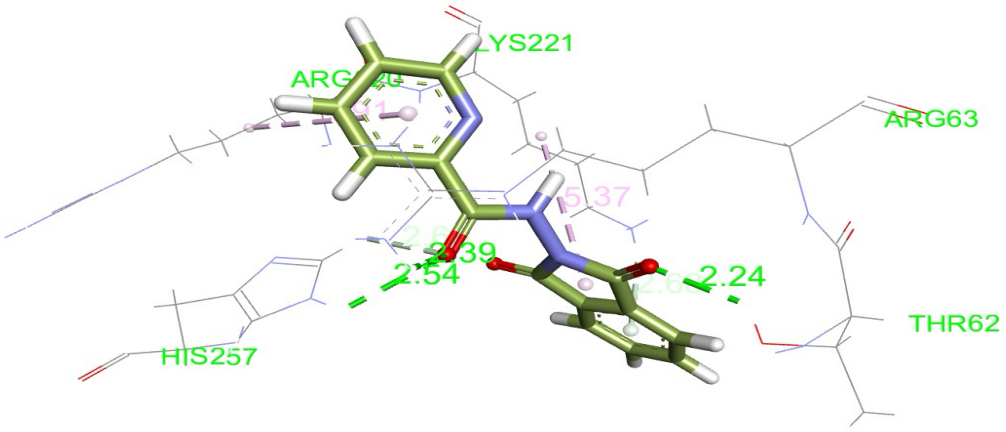

3E

Figure 3. Three-dimensional docking poses of ligands within bacterial protein 1AJ0 active site. (A) Co-crystal reference ligand orientation showing key interacting residues ARG A:63, ARG A:255, HIS A:257, and LYS A:221. (B) Compound 4 binding mode illustrating hydrogen bonding network with THR A:62, ARG A:63, and PHE A:188. (C) Compound 5 docking pose highlighting interactions with THR A:62, ARG A:63, HIS A:257, LYS A:221, and ARG A:255. (D) Compound 6 binding confirmation demonstrating hydrogen bonds with THR A:62, HIS A:257, ARG A:63, and ARG A:220. (E) Compound 7 optimal binding pose showing extensive interaction network including THR A:62, HIS A:257, ARG A:63 and aromatic stacking opportunities. Ligands are displayed in ball-and-sticky representation with carbon atoms in green, nitrogen in blue, oxygen in red, and hydrogen in white. Protein residues are shown as line with key residues labeled. Hydrogen bonds are depicted as green dashed lines with distance Ångströms. The three-dimensional docking poses presented in Figure 3 provided comprehensive visualization of Ligand accommodation within 1AJ0 binding pocket. Comparative analysis reveals progressive optimization of binding geometry from co-crystal ligand through compounds 4-7, with compound 7 demonstrating optimal spatial complementarity with active side architecture. The visualization confirms formation of critical hydrogen bonding networks while highlighting the importance of aromatic ring incorporation for enhanced protein-ligand recognition.

Structure-Activity Relationship Delineation

Docking results furnish valuable insights into structure-activity relationship governing picolinohydrazide derivative binding to 1AJ0 protein. Chain length extension from four carbons (compound 4) to five carbons (compound 6) yielding approved binding affinity, implying glutaryl moiety furnishes optimal geometrical complementarity. Aromatic ring incorporation into phthalic moiety (compound 7) precipitated most significant binding affinity improvement, demonstrating aromatic interactions perform critical roles stabilizing ligand protein assemblies [32]. Comparison between compound 4 and 5 highlights conformational flexibility importance, suggesting capable adapting multiple confirmation surpassed

enforced planarity importance. All synthesized compounds engage the three key hydrogen bonding residues (LYS A:221, HIS A:257, THR A:62), whereas co-crystal ligand interacted with merely two residues, appeared as significant contributor to improve binding affinity.

Conclusion

Our investigation successfully demonstrated synthesis, characterization, and computational assessment for four novel picolinohydrazide derivatives as potential antibacterial agents targeting bacterial protein 1AJ0. The synthetic pathway demonstrated efficiency and reproducibility delivering targeted compounds in moderate to satisfactory yield (50-62%). Comprehensive spectroscopic characterization employing ATR-FTIR, ^{1}H-NMR and ^{13}C-NMR verified all synthesized compound structure, providing definitive structural confirmation through multiple complementary analytical techniques.

Computational Docking investigations revealed all four synthesized derivatives (4-7) exhibited superior 1AJ0 protein binding affinities versus co-crystal reference, with binding energy enhancement spanning 17.4 to 31.5%. Compound 7, incorporating aromatic phthalic moiety, emerged as most promising candidate with -5.88 kcal/mol binding energy, representing substantial 31.5% enhancement beyond co-crystal reference (-4.47 kcal/mol). Enhanced binding affinity attributed to extensive hydrogen bonding network formation with key residues (LYS A:221, HIS A:257, THR A:62) supplemented by π-cation and π-alkyl interactions collectively supervising ligand protein assemblies.

Structure-activity relationship analysis disclosed aromatic moiety incorporation significant enhances binding affinity, likely through π-π stacking interactions and increase hydrophobic contacts. Additionally, optimally aliphatic linker region chain length (five carbons in compound 6) furnished improved geometrical complementarity with binding pocket versus shorter chains.

Conformational flexibility importance was demonstrated through saturated versus unsaturated derivative comparison, with flexible saturated chain exhibiting superior binding.

Our investigation findings suggest picolinohydrazide derivative represent promising scaffolds for developing novel antibacterial agents with enhanced bacterial protein targeting binding characteristics.

Clear structure-activity relationship identified herein furnish valuable guidance for future optimization initiatives aimed at developing compounds with even greater affinity and selectivity. However, these computational predictions require experimental binding study and antibacterial activity assay validation confirming therapeutic potential. Continued novel antibacterial agent development based on heterocyclic scaffolds remains critical priority in addressing global antimicrobial resistance challenge.

Acknowledgments

We gratefully acknowledge the College of Pharmacy, Department of Pharmaceutical Chemistry Tikrit University for their valuable support and contributions which significantly facilitated the advancement of this research and achievements of it is objectives.

Ethics Statements

The study did not need ethical approval from an ethics committee.

Conflict of Interest

The authors declare no conflict of interest.

Author Contribution

The authors confirm contribution to the paper as follows: supplying of Picolinic acid, study design, supervision on the progress of the reactions, interpretation of ATR-FTIR, ^{1}H-NMR and ^{13}C-NMR and interpretation of docking results: Ali H. Abbas; interpretation of the results and providing essential references: Yahya Saad Yaseen, Mostafa Fayez Tawfeeq and Yaseen Saleem Hamdoon. All authors reviewed the results and approved the final version of the manuscript.

References

1. Silver LL. Challenges of antibacterial discovery. *Clin Microbiol Rev.* 2011;24(1):71–109. DOI: 10.1128/CMR.00030-10
2. Payne DJ, Gwynn MN, Holmes DJ, Pompliano DL. Drugs for bad bugs: confronting the challenges of antibacterial discovery. *Nat Rev Drug Discov.* 2007;6(1):29–40. DOI: 10.1038/nrd2201
3. Hughes JP, Rees S, Kalindjian SB, Philpott KL. Principles of early drug discovery. *Br J Pharmacol.* 2011;162(6):1239–1249. DOI: 10.1111/j.1476-5381.2010.01127.x
4. Vitaku E, Smith DT, Njardarson JT. Analysis of the structural diversity, substitution patterns, and frequency of nitrogen heterocycles among U.S. FDA approved pharmaceuticals. *J Med Chem.* 2014;57(24):10257–10274. DOI: 10.1021/jm501100b
5. Kerru N, Gummidi L, Maddila S, Gangu KK, Jonnalagadda SB. A review on recent advances in nitrogen-containing molecules and their biological applications. *Molecules.* 2020;25(8):1909. DOI: 10.3390/molecules25081909
6. Altaf AA, Shahzad A, Gul Z, Rasool N, Badshah A, Lal B, et al. A review on the medicinal importance of pyridine derivatives. *J Drug Des Med Chem.* 2015;1(1):1–11. DOI: 10.11648/j.jddmc.20150101.11
7. Popiołek Ł. Hydrazide-hydrazones as potential antimicrobial agents: overview of the literature since 2010. *Med Chem Res.* 2017;26(2):287–301. DOI: 10.1007/s00044-016-1766-4
8. Pinzi L, Rastelli G. Molecular docking: shifting paradigms in drug discovery. *Int J Mol Sci.* 2019;20(18):4331. DOI: 10.3390/ijms20184331
9. Torres PHM, Sodero ACR, Jofily P, Silva FP Jr. Key topics in molecular docking for drug design. *Int J Mol Sci.* 2019;20(18):4574. DOI: 10.3390/ijms20184574
10. Meng XY, Zhang HX, Mezei M, Cui M. Molecular docking: a powerful approach for structure-based drug discovery. *Curr Comput Aided Drug Des.* 2011;7(2):146–157. DOI: 10.2174/157340911795677602
11. Anderson AC. The process of structure-based drug design. *Chem Biol.* 2003;10(9):787–797. DOI: 10.1016/j.chembiol.2003.09.002
12. Sliwoski G, Kothiwale S, Meiler J, Lowe EW Jr. Computational methods in drug discovery. *Pharmacol Rev.* 2014;66(1):334–395. DOI: 10.1124/pr.112.007336
13. Ferreira LG, Dos Santos RN, Oliva G, Andricopulo AD. Molecular docking and structure-based drug design strategies. *Molecules.* 2015;20(7):13384–13421. DOI: 10.3390/molecules200713384
14. Reddy PN, Srirama K, Dirisala VR. An update on clinical burden, diagnostic tools, and therapeutic options of *Staphylococcus aureus*. *Infect Dis.* 2017;10:1179916117703999. DOI: 10.1177/1179916117703999
15. Wright GD. Molecular mechanisms of antibiotic resistance. *Chem Commun.* 2011;47(14):4055–4061. DOI: 10.1039/c0cc05111j
16. Rollas S, Küçükgüzel SG. Biological activities of hydrazone derivatives. *Molecules.* 2007;12(8):1910–1939. DOI: 10.3390/12081910
17. Naim MJ, Alam O, Nawaz F, Alam MJ, Alam P. Current status of pyrazole and its biological activities. *J Pharm Bioallied Sci.* 2016;8(1):2–17. DOI: 10.4103/0975-7406.171700
18. Verma G, Marella A, Shaquiquzzaman M, Akhtar M, Ali MR, Alam MM. A review exploring therapeutic worth of 1,2,4-triazole scaffold. *J Pharm Bioallied Sci.*

2014;6(2):69–80.
DOI: 10.4103/0975-7406.129170
19. Molecular Operating Environment (MOE), 2022.02. Chemical Computing Group ULC, Montreal, QC, Canada, 2022.
20. Kitchen DB, Decornez H, Furr JR, Bajorath J. Docking and scoring in virtual screening for drug discovery. *Nat Rev Drug Discov.* 2004;3(11):935–949. DOI: 10.1038/nrd1549
21. Mohan V, Gibbs AC, Cummings MD, Jaeger EP, DesJarlais RL. Docking: successes and challenges. *Curr Pharm Des.* 2005;11(3):323–333. DOI: 10.2174/1381612053382106
22. Böhm HJ. Development of a simple empirical scoring function. *J Comput Aided Mol Des.* 1994;8(3):243–256. DOI: 10.1007/BF00124429
23. Labute P. The generalized Born/volume integral implicit solvent model. *J Comput Chem.* 2008;29(10):1693–1698. DOI: 10.1002/jcc.20933
24. Kontoyianni M, McClellan LM, Sokol GS. Evaluation of docking performance. *J Med Chem.* 2004;47(3):558–565. DOI: 10.1021/jm0302997
25. Bissantz C, Kuhn B, Stahl M. A medicinal chemist's guide to molecular interactions. *J Med Chem.* 2010;53(14):5061–5084. DOI: 10.1021/jm100112j
26. Otera J, Nishikido J. *Esterification: Methods, Reactions, and Applications.* 2nd ed. Wiley-VCH; 2010.
27. Rollas S, Küçükgüzel SG. Biological activities of hydrazone derivatives. *Molecules.* 2007;12(8):1910–1939. DOI: 10.3390/12081910
28. Warren GL, Andrews CW, Capelli AM, et al. A critical assessment of docking programs. *J Med Chem.* 2006;49(20):5912–5931. DOI: 10.1021/jm050362n
29. Meyer EA, Castellano RK, Diederich F. Interactions with aromatic rings. *Angew Chem Int Ed.* 2003;42(11):1210–1250. DOI: 10.1002/anie.200390319
30. Böhm HJ, Klebe G. Molecular recognition in protein–ligand complexes. *Angew Chem Int Ed.* 1996;35(22):2588–2614. DOI: 10.1002/anie.199625881
31. Martinez CR, Iverson BL. Rethinking the term "π-stacking". *Chem Sci.* 2012;3(7):2191–2201. DOI: 10.1039/C2SC20045G
32. Brown DG, Boström J. Synthetic methodologies in medicinal chemistry. *J Med Chem.* 2016;59(10):4443–4458. DOI: 10.1021/acs.jmedchem.5b01409